GENERALISED TECHNIQUE FOR THE SIMULATION OF NEAR FIELD ANTENNA MEASUREMENTS

C. Mitchelson, S.F. Gregson
BAE SYSTEMS Avionics Group, UK

ABSTRACT

The recent development of a probe-corrected poly-planar near field antenna measurement technique [1] necessitated the development of general-purpose simulation tools that could be used within the validation campaign. This paper demonstrates through numerical simulation and experimental measurement a new, generally applicable, near field simulation tool based on a hybrid physical-optics (PO) reaction-theorem (RT) formulation that is capable of supplying simulations of any of the near field measurement systems that are currently found in use today. This is of interest because it enables 1) an engineer to plan and optimise a measurement campaign before committing valuable facility time, 2) error terms within the facility error budget can be accurately determined, 3) the probe-correction algorithms that form a crucial constituent of any transformation routine to be carefully verified.

1. INTRODUCTION

Any near field measurement can essentially be simulated by evaluating the complex coupling coefficient between the antenna under test (AUT) and the near field probe at each point over the simulated acquisition surface for each sampled polarisation for the frequency at which the measurement is to be taken. In principle then, it would be possible to obtain the mutual coupling coefficient (S_{21}) between the AUT and the scanning probe from a three-dimensional electromagnetic full-wave solver for each of the positions at which near field samples are to be recorded. This approach would have the advantage of potentially introducing the least number of assumptions and approximations, and therefore could, in theory, yield the most accurate predications.

Unfortunately, although many solvers are available employing say, the finite difference time domain (FDTD), or the finite element methods (FEM), *etc.* they are generally thought to be inappropriate for simulating problem spaces as electrically large as those needed to enclose a complete near field measurement system. This is a direct consequence of the extended processing times and the amount of computer resources required. Hence, recourse to alternative less general, but more efficient, techniques becomes unavoidable. However, matters are complicated by recognising that, the poly-planar configuration is capable of yielding full 4π steradian far field antenna patterns. Thus, the problems of simulating the near field measurement are perhaps more akin to those associated with the simulation of cylindrical or spherical measurement configurations necessitating the harnessing of a very general approach.

2. METHOD

Provided that the antennas, and the circuits in which they are placed, including the source and load, are reciprocal then the mutual coupling between two antennas can be found from knowledge of the fields radiated by these antennas in isolation and from the reaction theorem. If the fields radiated by an antenna are known over a convenient, arbitrary, closed surface that surrounds the antenna, then the field radiated by this antenna at any point in the region of space outside this surface can be obtained from the Kirchhoff-Huygens principal. As illustrated schematically below in Figure 1, if the Kirchhoff-Huygens formula is used to obtain the fields radiated by antenna 1 over a closed surface that surrounds antenna 2, provided that the fields radiated by antenna 2 are also known over this surface, then the surface integral form of the reaction theorem can be used to calculate the mutual impedance between these antennas. The mutual admittance between the antennas can then be found from the mutual impedance. These admittances can be used to populate an admittance matrix from which the equivalent normalised scattering matrix can be easily obtained. The transmission scattering coefficient, when evaluated with the two antennas suitably displaced can be recognised as constituting a single sampling node within a near field measurement. By repeating this for every point in the near field measurement a full acquisition can be constructed. As the displacement and orientation of the coupled antenna system can be chosen arbitrarily, provided only that the enclosing surfaces do not intersect, any near field (or quasi far field) measurement system can be simulated.

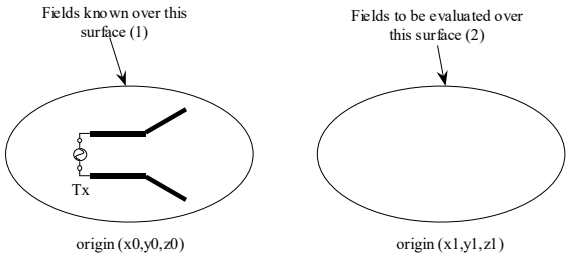

Figure 1: Geometry of KH-RT

These measurement simulations include artefacts resulting from the vector pattern function, *i.e.* the directivity, of the scanning near field probe. This is especially important when simulating measurements taken using a planar, or poly-planar, facility, the effect includes something similar to a direct multiplication of the probe pattern with the antenna pattern in the far field. This results from the convolution of the near field pattern of the probe with that of the AUT, which may be visualised directly from the mechanical operation of the scanner. It is not usually possible to neglect these effects in a planar range because of the large angles of validity required and the short

measurement distance. Hence, simulations produced from this procedure can be used to rigorously verify the corrections made for the modal receiving coefficients (*e.g.* plane wave) of the scanning probe during the near field to far field transformation process. The following sections present the details of this simulation technique.

Field Propagation: Kirchhoff-Huygens Principal

The Kirchhoff-Huygens principal is a powerful technique for determining the field in a source free region outside an enclosing surface from knowledge of the field distribution over that surface. It is applicable to arbitrary shaped "apertures" over which both the electric and magnetic fields are prescribed. When expressed mathematically, the vector electric field at a point *P*, radiated by a closed Huygens surface *S* is [2],

$$\underline{E}_p = \frac{1}{4\pi}\int_S \left[-j\omega\mu\left(\hat{n}\times\underline{H}\right)\psi + \left(\hat{n}\times\underline{E}\right)\times\nabla_0\psi + \left(\hat{n}\cdot\underline{E}\right)\nabla_0\psi\right]ds_0 \quad (1)$$

Similarly, the magnetic field at a point *P*, radiated by a closed Huygens surface *S* is,

$$\underline{H}_p = \frac{1}{4\pi}\int_S \left[j\omega\varepsilon\left(\hat{n}\times\underline{E}\right)\psi + \left(\hat{n}\times\underline{H}\right)\times\nabla_0\psi + \left(\hat{n}\cdot\underline{H}\right)\nabla_0\psi\right]ds_0 \quad (2)$$

Here, $\underline{E}$ and $\underline{H}$ are taken to denote the electric and magnetic fields respectively over the enclosing surface, ψ denotes the first order spherical wave function (which is also known as the free space Green's function),

$$\psi = \frac{e^{-jk_0r'}}{r'} \quad (3)$$

where r' is the displacement of the field point from the elemental source and is related to the co-ordinates of the elemental Huygens source $\underline{r}_0$ and the co-ordinates of the field point $\underline{r}$ by, $r' = |r\text{-}\underline{r}_0|$. ω is the angular frequency, k_0 is the free space propagation constant, and $\underline{n}$ is the outward pointing unit surface normal. ε and μ are the permittivity and permeability of the medium respectively through which the field is propagating. The differential vector operator ∇_0 expressed in the source co-ordinate system acting on ψ can easily be shown to be,

$$\nabla_0\psi = \left(jk_0 + \frac{1}{r'}\right)\underline{\hat{r}}'\psi \quad (4)$$

Thus, the Kirchhoff formula for the vector electric and magnetic vector fields at a point *p* anywhere outside the volume of space enclosed by the bounding surface *S* can be expressed as,

$$\underline{E}_p = \frac{1}{4\pi}\int_S \left[-j\omega\mu\left(\hat{n}\times\underline{H}\right) + \left\{\left(\underline{\hat{n}}\times\underline{E}\right)\times\underline{\hat{r}}' + \left(\hat{n}\cdot\underline{E}\right)\underline{\hat{r}}'\right\}\left(jk_0 + \frac{1}{r'}\right)\right]\frac{e^{-jk_0r'}}{r'}ds_0 \quad (5)$$

and,

$$\underline{H}_p = \frac{1}{4\pi}\int_S \left[j\omega\varepsilon\left(\hat{n}\times\underline{E}\right) + \left\{\left(\hat{n}\times\underline{H}\right)\times\underline{\hat{r}}' + \left(\hat{n}\cdot\underline{H}\right)\underline{\hat{r}}'\right\}\left(jk_0 + \frac{1}{r'}\right)\right]\frac{e^{-jk_0r'}}{r'}ds_0 \quad (6)$$

Thus, if the electric and magnetic vector fields are known over surface 1, the corresponding fields over surface 2 can be determined by evaluating expressions (5) and (6). Unfortunately, the utilisation of numerical integration techniques becomes inevitable for all but the most elementary cases.

Mutual Impedance: Reaction Theorem

Provided that the electric and magnetic field vectors ($\underline{E}_1$, $\underline{H}_1$) and ($\underline{E}_2$, $\underline{H}_2$) are of the same frequency and monochromatic then the mutual impedance, Z_{21}, between antenna 1 and 2 in the environment described by ε, μ can be expressed, from the reaction theorem, in terms of a surface integration as [3],

$$Z_{21} = \frac{V_{21}}{I_{11}} = -\frac{1}{I_{11}I_{22}}\int_{S_2}\left(\underline{E}_2\times\underline{H}_1 - \underline{E}_1\times\underline{H}_2\right)\cdot\hat{\underline{n}}\,ds \quad (7)$$

Again, $\underline{n}$ is taken to denote the outward pointing surface unit normal. The subscript 1 denotes parameters associated with antenna 1 whilst the subscript 2 denotes quantities associated with antenna 2, *i.e.* S_2 is a surface that encloses antenna 2, but not antenna 1. Here, I_{11} is the terminal current of antenna 1 when it transmits and similarly, I_{22} is the terminal current of antenna 2 when it transmits. From reciprocity, the mutual impedance, $Z_{12} = Z_{21}$, and is related to the coupling between two antennas. Clearly then the mutual impedance will also be a function of the displacement between the antennas, their relative orientations, and their respective polarisation properties.

The terminal current of these transmitting antennas, I_{11} and I_{22} can be obtained from the knowledge of the power injected at the port, P_1 and P_2 which is typically taken to be unity, and is specified within the modelling tool, and the port impedance Z_1 or Z_2 using,

$$I_{11} = \sqrt{\frac{P_1}{Z_1}} \quad (8)$$

If for example, a waveguide port has been used to stimulate the problem, the impedance Z_1 can be taken to be the impedance of the mode excited at that port. At 10 GHz, the TE_{10} mode is the only mode to propagate in the waveguide sections of the waveguide horn and the waveguide probe. Thus, the impedance at each port can be taken to be,

$$Z_1 = Z_2 = Z_{TE} = \frac{k}{\beta}\sqrt{\frac{\mu}{\varepsilon}} \quad (9)$$

Where,

$$k = \omega\sqrt{\mu\varepsilon} \quad (10)$$

and

$$\beta = \sqrt{k^2 - \left(\frac{\pi}{a}\right)^2} \quad (11)$$

Derivation of Two-Port Scattering Matrix

The self-impedance Z_{11} and Z_{22} can be obtained in many ways. However, they are perhaps most easily obtained from whichever three dimensional full-wave electromagnetic solver was used to obtain the radiated fields from the isolated antennas. As an admittance is

merely the reciprocal of an impedance, an admittance matrix [Y] representing this two port coupled systems can be readily populated so that,

$$[Y]=\begin{bmatrix} Y_{11} & Y_{12} \\ Y_{21} & Y_{22} \end{bmatrix} \qquad (12)$$

It is well known that the re-normalised scattering matrix, [S_Ω], can be calculated from this admittance matrix and is used to describe what fraction of the signal is transmitted, or reflected at each port,

$$[S_\Omega]=\sqrt{[Y_\Omega]}([Z]-[Z_\Omega])([Z]+[Z_\Omega])^{-1}\sqrt{[Z_\Omega]} \quad (13)$$

Here, $[Y_\Omega] = ([Z_\Omega])^{-1}$ and is a diagonal matrix with the desired normalising admittance as the diagonal entries, *i.e.* the admittance of the attached transmission line which in this case will be equal to the port impedance $Z_1 = Z_2 = Z_{TE}$. This can be expressed mathematically as,

$$[Y_\Omega]=Y_\Omega\delta_{ij} \qquad (14)$$

With $\delta_{i,j}$, denoting the Kronecker delta where i and j are positive integers,

$$\delta_{ij}=\begin{cases} 1 & (i=j) \\ 0 & (i\neq j) \end{cases} \qquad (15)$$

The elements $S_{1,2} = S_{2,1}$ of [S_Ω] are the complex transmission coefficients for the coupled antenna system which are taken to represent a single point in the near field measurement. This then completes what is essentially a method of moments analysis of this system. The near field measurement simulation algorithm can be summarised as follows.

1. Use equations 5 and 6 to translate the fields of antenna 1 to antenna 2.
2. Use equation 7 to evaluate the mutual impedance and thus the mutual admittance.
3. Populate the admittance matrix for the two-antenna system.
4. Use equation 13 to determine the complex mutual coupling coefficient
5. Repeat steps 1-4 inclusive for each sample point in the near field scan.
6. Rotate the probe to simulate the sampling of a second orthogonal near field component and repeat step 1-5 inclusive to generate a second scan and thus complete the near field acquisition.

The generality of this treatment can be highlighted by observing that the mutual coupling coefficients of a finite m-element array can also be obtained from this procedure by merely populating a larger, *i.e.* m by m, admittance matrix.

3. PRELIMINARY VERIFICATION

The amount of power coupled between a pair of polarisation matched loss-less dipoles that are perfectly matched to their respective source and load, and that are in the far field of one another can be obtained from the well known Friis transmission formula.

$$\frac{P_R}{P_T}=\left(\frac{\lambda}{4\pi R}\right)^2 G_T G_R \qquad (16)$$

Conversely, the mutual coupling coefficient can be obtained by taking the $\underline{E}$ and $\underline{H}$-fields from a half-wavelength dipole from a full wave-solver, microwave studio in this case, and using the PO-RT algorithm set out above. As the antennas that are transmitting and receiving are of exactly the same design $G_R = G_T$. The gain of the dipole at 10 GHz along the x-axis was approximately 2.16dB. Figure 2 below contains a comparison of the mutual coupling obtained using these two contrasting methods. From inspection, it is clear that the agreement is encouraging with differences only becoming more pronounced as the separation becomes smaller, *i.e.* in the region where the far field approximation within the Friis transmission equation is most significant.

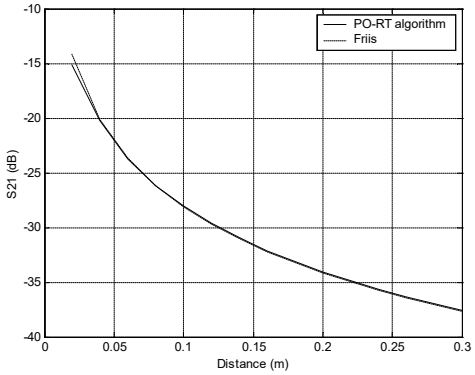

Figure 2: Mutual couping between adjacent dipoles

4. NEAR FIELD MEASUREMENT SIMULATION

Figure 3 below contains a schematic representation of the near field probe and a standard gain horn (SGH) which was used as an AUT. The faint grey ellipsoidal surface that can be seen to enclose these instruments represents the Huygens surface that was used with the PO-RT computational electromagnetic simulation (CEM) simulation. The scanning probe consisted of an Orbit RF AL-2000-PRB-90 open-ended rectangular waveguide probe combined with a surface wave absorbing (SWAM) cone that was designed to minimise reflections from the mechanical interface located towards the rear of the probe. A detailed description of the modelling and verification thereof can be found within the literature [4]. Again similarly good agreement was attained between the CEM model of the SGH and measurements taken using a compact antenna test range (CATR).

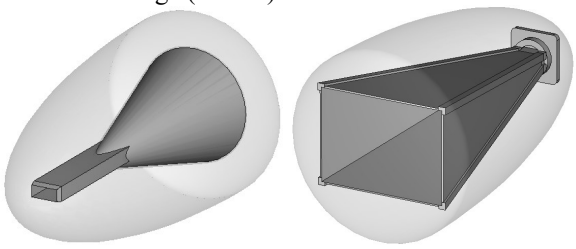

Figure 3: Near field probe and AUT (SGH)

A near field measurement of the SGH was taken using a planar near field antenna test range (PNATR). The acquisition window was chosen to be ±0.8m in the x-y plane whilst the distance between the SGH and the near field probe in the z-direction was set at 10.0 cm,

i.e. approximately 3 wavelengths (3λ) at 10.0 GHz. This separation insured that the probe was outside the reactive near field, made the first order truncation angle as large as possible (≈±83° in azimuth and elevation) and attempted to minimise the detrimental effects arising from multiple reflections that can be induced between the AUT and the scanning probe. Although phenomena arising from the first two of these effects will be included within the measurement simulation, multiple reflections between the AUT and the probe are ignored.

The separation between adjacent measurement points was one half wavelength as this satisfied the Nyquist sampling criteria, and in the absence of errors in the position at which measurements are taken, will guarantee alias free far field patterns over the entire forward half-space. The SGH was installed in the rage so that it was principally "*y*-polarised" with respect to the axes of the near field range.

5. RESULTS

Figure 4 and 5 below contain a comparison of horizontal and vertical cuts through the simulated near field measurement and the actual near field measurement.

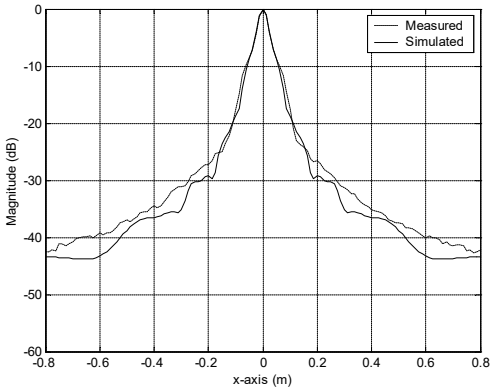

Figure 4: Near field cut in x-axis

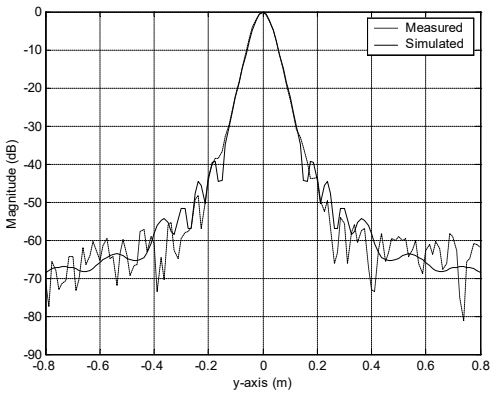

Figure 5: Near field cut in y-axis

The agreement between the simulation and measurement is encouraging in both planes and it suggests that the simulation code is capable of creating a simulation of a measurement taken on a near-field range. In particular, the cut in the y-axis, Figure 5, where there is less energy as you move away from the centre shows very good agreement. It is only when the magnitude of the coupling is at lower levels, *i.e.* < -40dB, that the characteristics of the two lines begin to diverge.

Inevitably, the measurement contains uncertainties arising from imperfections in alignment (both in translation, *x*, *y*, *z* and rotation in azimuth, elevation, roll), multi-path (scattering from the chamber walls and the frame of the robotic positioner), multiple reflections between the antenna and the probe, and imperfections in the manufacture of both the probe and AUT. None of these error terms are included within the near field simulation.

6. DISCUSSION AND CONCLUSIONS

This paper has introduced and demonstrated initial empirical verification a general-purpose method for the simulation of measurements taken using *any* of the near field geometries available today that includes provision for probe pattern effects which are often one of the largest terms in the facility level error budget.

Unfortunately, the evaluation of the transmission coefficient S_{21} requires the computationally expensive evaluation of a sextuple integration to obtain each near field sample point. However, the simulation of an entire near field measurement constitutes a coarsely granular problem. Specifically, each sampling node can be evaluated independently of every other sampling node and in this way, provided only that a sufficiently large array, *i.e.* cluster, of computers is available, the total processing time is in principal equal to the time taken to evaluate a single measurement point.

Finally, it has also been highlighted that this technique neither relies on the modal expansion method for the representation of electromagnetic waves nor does it utilise inversions of conventional probe pattern correction algorithms. Thus, it provides an independent approach to the verification of existing near field to far field transformation algorithms.

REFERENCES

1. S.F. Gregson, C.G. Parini, J. McCormick, "Wide Angle Antenna Pattern Measurements Using a Poly-Planar Near Field Technique", International Conference on Antennas and Propagation, 2003, Exeter.
2. R.H. Clarke, J. Brown, "Diffraction Theory and Antennas", Ellis Horwood Ltd., 1980, pp 227.
3. J.H. Richmond, "A Reaction Theorem and Its Application to Antenna Impedance Calculations", IRE Trans. Antenna and Propagation, 1961, pp. 515-320.
4. R.W. Lyon, S.F. Gregson, C Mitchelson, J. McCormick, "Computational Electromagnetic Modelling of a Probe Employed in Planar Near Field Antenna Measurements", ICAP 2003, Exeter.